Research Article | Vol. 30, No. 12 / 6 Jun 2022 / Optics Express 21746
Optics EXPRESS

Blurred spectral images restoration technology for AOTF imaging spectrometer based on dual-path architecture

PENGWEI ZHOU,[1,*] YING WANG,[2] ZHUOER HE,[1] HUASHENG XU,[1] YI LI,[1] AND DONG YAO[3]

[1] College of Optical and Electronic Technology, China Jiliang University, Hangzhou, Zhejiang 310018, China
[2] School of Information Engineering, Hangzhou Dianzi University, Hangzhou, Zhejiang 311305, China
[3] Key Laboratory of Airborne Optical Imaging and Measurement, Changchun Institute of Optics, Fine Mechanics and Physics, Chinese Academy of Science, Changchun, Jilin 130033, China
[*] zhoupw@cjlu.edu.cn

Abstract: The acousto-optic tunable filter (AOTF) imaging spectrometer is a staring-type instrument that acquires spectral images of different bands asynchronously and sequentially, and is susceptible to platform jitter and target motion. When the integration time of the detector increases, serious spectral images degradation occurs along with a large band-to-band misregistration. The dual-path optical configuration, capable of simultaneously acquiring diffracted and undiffracted beams of AOTF, has been shown to be effective in solving the problem of band-to band misregistration. Hence by solving the remaining spectral image degradation problems, the application range of AOTF will transcend the previous limitation. Therefore, this paper presents a new, to the best of our knowledge, method of capturing a series of short-exposure undiffracted beam images to calculate the blur kernel of the diffracted spectral images, since the high-intensity characteristics of the undiffracted beam can also be exploited in the dual-path system. The paper starts with analyzing the impact of the platform on spectral images, and then demonstrates the development and calibration of a dual-path based spectral image deblurring method. Finally, laboratory experiment verifies that the resulting blur kernel can be effectively used for spectral image restoration, thus demonstrating the robustness of this technique.

1. Introduction

Acousto-optic tunable filter is a fast and arbitrary band tuning device covering wide wavelength range [1]. Taking advantage of staring imaging, an AOTF imaging spectrometer allows tracking of moving targets or continuous observations of specific regions of interest. However, to obtain the full spectral data cube, it needs to asynchronously and sequentially acquires spectral images of different bands. Due to this time-consuming nature, AOTF imaging spectrometer is susceptible to platform jitter. Therefore, the prior applications of AOTF normally have high requirement on the stationarity of platforms [2]. The main reason is that the relatively high ground motion speed of non-geostationary orbit or straight wing aircraft leads to large band-to-band misregistration as well as serious spectral images blur. Spectral images from different bands are often difficult to achieve accurate band-to-band registration because of poor correlation and low SNR. Previous work [3] has shown that a technique of a dual-path system, could improve the band-to-band registration accuracy robustly, by deriving misregistration information from undiffracted beams of AOTF, as shown in Fig. 1(a). Compared with diffracted spectral beam path, the undiffracted beam's intensity is constant when tuning AOTF. After calibrating the matching relationship between each spectral image band and the undiffracted image, the spectral mismatch relationship between two different bands can be transformed to solving the mismatch relationship of two

#459972 https://doi.org/10.1364/OE.459972
Journal © 2022 Received 5 Apr 2022; revised 25 May 2022; accepted 25 May 2022; published 1 Jun 2022

Optics EXPRESS

highly correlated undiffracted beam images. However, as shown in Fig. 1(b), when an identical point target is captured sequentially at different bands, the PSF blur kernel caused by the platform motion may be large in scale and present different shapes. Hence, it is difficult to explore a reasonable registration position for these two blurred spectral images, which can be regarded as the inevitable band misregistration as a consequence of different blur kernels. In addition, blurred spectral images are still difficult to restore robustly and accurately due to the insufficient motion blur kernel. Therefore, even in common geosynchronous orbits satellites or helicopters that are already relatively stationary to the ground, it is expected that the satellites will have a higher attitude stability, and the helicopter will be equipped with a high-precision stabilization platform. Such strict environmental requirements restrict the aerospace application of AOTF imaging spectrometers only to landers so far. Therefore, the blur of AOTF spectral images due to relative motion is a key issue demanding prompt solution.

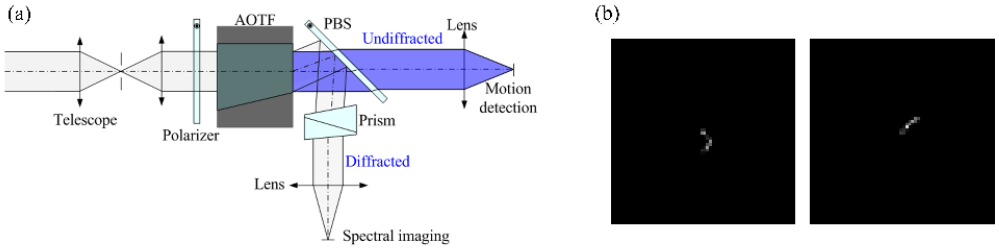

Fig. 1. (a)Schematic of dual-path AOTF imaging spectrometer. (b) A same point target blurred by two different PSF kernels.

If the focus is on earth observation from space, three possible modes of AOTF imaging spectrometer have been observed in Fig. 2, which are nadir-pointing from geostationary earth orbit (GEO), nadir-pointing from non-geostationary orbit, and specified areas pointing from non-geostationary agile earth observing satellite (AEOS) [4].

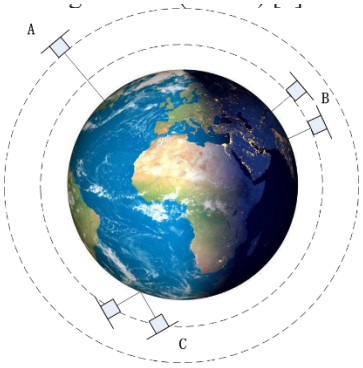

Fig. 2. Three observation modes of AOTF imaging spectrometer in earth remote sensing.

Comparatively, nadir-staring from GEO satellite is recognized as the most promising application [5]. The attitude stability of nadir-pointing satellite is usually 10^{-3}~10^{-4} degrees/s, and some platforms can reach 10^{-6} degrees/s (Landsat 4 satellite). If the spectrometer's integration time per band is set to 100 milliseconds for higher signal-to-noise ratio (SNR), 5 seconds is required to scan 50 spectral bands. For a GEO spectrometer with the ground sample resolution (GSD) of 10 meters, high attitude stability of 10^{-6} degrees/s ensures negligible spectral image blur (0.0063 pixels) and small band to band displacement (0.3142 pixels). However, lower stability of

Optics EXPRESS

5×10^{-4} degrees/s will enlarge the spectral image blur to 3.1416 pixels, which also increase the band-to-band displacement to 157.0796 pixels. Therefore, a platform with higher stability seems a necessity to improve image and spectra quality on geostationary earth orbit.

In the case of nadir-pointing from non-geostationary orbit, which possesses the global observation capability, image blur and spectral misregistration presents to be more severe. For example, when the altitude of the satellite is 600 km, the average satellite ground speed of is generally around 7 Km/s. Under the same GSD condition of 10 m, image blur and spectral misregistration reach up to 70 pixels and 3500 pixels respectively, even when attitude changes are ignored. Due to the large blur of the image, it is difficult to find an accurate method for restoration. Meanwhile, such a large band mismatch also leads to no overlapping area between the first and last bands, and it is impossible to obtain a complete spectral curve. Consequently, it is crucial to avoid the sub-satellite point mode in non-geostationary orbit.

Therefore, the last mode is anticipated to achieve global observation, which is the region-locked observation that has been popular in recent years. It relies on the attitude adjustment ability of AEOS to lock a specific area. At first glance, it seems to be very experimental for staring-type instruments. However, the orbit and attitude control of AEOS is more complicated and difficult, and many literatures currently use 0.01 degrees/s [6] as the attitude stability accuracy. Since AOTF takes a long time to acquire all spectral images, the imaging quality under such a low attitude stability needs to be further evaluated. In addition, concerning that the angle of the boresight will change with the movement of the satellite, it is also valuable to emphasize on the inconsistency pixel shift in different image area. Coupled with the fact that the earth is a curved surface, the problem is more complicated and requires accurate model analysis.

We first establish the OXYZ coordinate system in Fig. 3(a), which corresponds to the earth centered earth fixed coordinates defined by the World Geodetic System 1984 (WGS84) standard. The satellite's centroid orbit coordinate system (O'XoYoZo) is also shown, whose Zo axis points to Earth's center, and Xo axis points to the direction of satellite velocity in the orbital plane. The position and velocity vector of the satellite at a specific moment can be given by the Satellite Tool Kit (STK) software according to the principle of orbital dynamics when the orbit is set. Therefore, the transformation matrix T1 from the satellite's centroid orbit coordinate system to WGS84 system can be calculated. Assuming that the imaging spectrometer coordinate system and the satellite body coordinate system have the same direction. Therefore, when the satellite at S points to a square region of interest, whose center point is defined as P, and the midpoint of one side is defined as M, the satellite attitude should be adjusted by rotating body to a specific angle. Thus, the satellite attitude angle is solvable. The scalar product of the vectors SP and SM determines the x-axis direction of the satellite body, while the z-axis direction of the satellite body is determined by SP, and the y-axis is identified by the right-hand rule. As a result, based on this solvable angle, the transformation T2 from the satellite's body coordinate system to the satellite centroid orbit coordinate system can also be obtained. Finally, it is possible to convert the light vectors under the imaging spectrometer system into the WGS84 coordinate system, and then the projection points of all rays can be determined by calculating the intersection of straight lines and ellipses. Therefore, when the satellite points to a specific area at different positions, there is only one suitable attitude. However, due to the attitude control error, the position of the ray's projection at different times will change.

This simulation hypothesizes that the AOTF imaging spectrometer equipped in a satellite having a circular orbit with height of 600 kilometers. The orbital inclination and the right ascension of the ascending node are assumed to be 100 degrees and −100 degrees, respectively. The start time when the satellite passes through the ascending node is set to 1 Jul 2007 12:00:00.000 UTCG. Then, the STK software is used to simulate this classical two-body system, which outputs the satellite's position vector and velocity vector parameters at 10 ms time intervals. The spectrometer is presumed to have a detector array of 256×256 pixels, and a GSD of 10 meters.

Optics EXPRESS

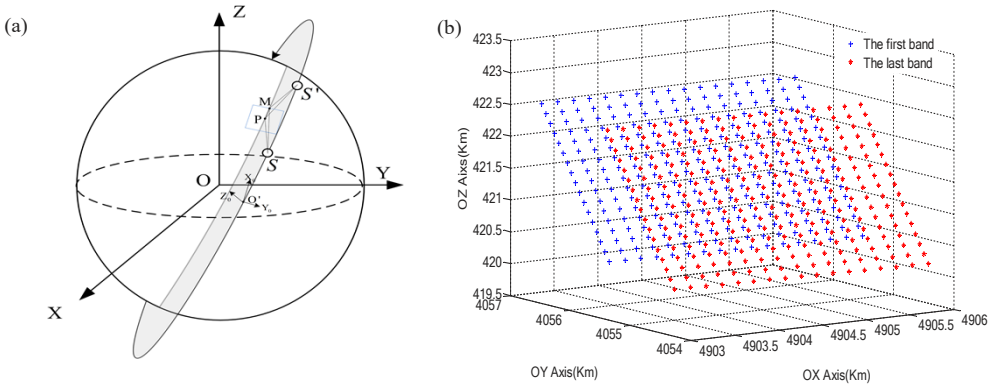

Fig. 3. (a) Schematic diagram of region-locked observation under the earth centered earth fixed (ECEF) coordinates (b) Projection of the first and last bands on the earth's surface in the WGS84 coordinate system.

Assume that the spectral image of the first band is acquired using the spectrometer pointing to nadir, when the satellite passes through a certain area. Subsequently, the satellite attitude is adjusted continuously to staring at this square region. Thus, the projection positions of each pixel can be calculated on the earth's surface in WGS84 coordinate system at 0 ms and 5000 ms. Figure 3(b) shows the positions of the first and last bands on the earth's surface, when the attitude stability accuracy is 0.01 degrees/s and pointing accuracy is 0.05 degrees, which is based on ASNARO-2 agile satellite. The figure shows the imaging coordinates corresponding to every 16 pixels on the detector. Among them, blue points represent the first band, and red points represents the 50th band.

Figure 4(a) shows the band-to-band misregistration between first and last spectral bands, which converts position difference values in Fig. 3(b) to pixel scale. The image shift varies between 73.7 pixels and 74.7 pixels in different image region, leading to an image motion difference of about one pixel. This difference is mainly due to the combined effects of unstable attitude, distance change and observation angle variation when the satellite is moving. Even though a small inconsistent image shift exists, the dual-path system is still effective. If only the registration of two unblurred undiffracted images is considered, there are some algorithms invariants to the image rotation, affine transformations and viewpoint change in matching features. For example, the scale-invariant feature transform (SIFT) [7] is perfectly suitable for solving the registration relationship of two undiffracted beam images captured when attitude, viewing angle and distance changes. Hence, the band-to-band misregistration with perspective distortion is resolvable. However, in the region-locked observation mode, the degradation of the spectral image during the integration time is still a pending problem. As shown in Fig. 4(b), the image blur caused by the attitude instability in the first band reaches 1.48 pixels, which causes the degradation of spectral image quality. According to the previous analyses, this will also inevitably engender band-to-band misregistration caused by different PSFs. Since the integration time and blur kernel of the undiffracted beam path are also the same as those of the diffracted beam, the credibility of band-to-band displacements calculated from the blurred undiffracted images is also reduced. Therefore, image blurring is the core problem that limits the application of AOTF imaging spectrometers on low-orbit agile satellites, which will be more serious when the spatial resolution is higher. Fortunately, the spectral image shows a good consistency of motion blur, and the motion difference is within 0.01 pixel. Therefore, it is possible to improve image quality by image restoration.

Optics EXPRESS

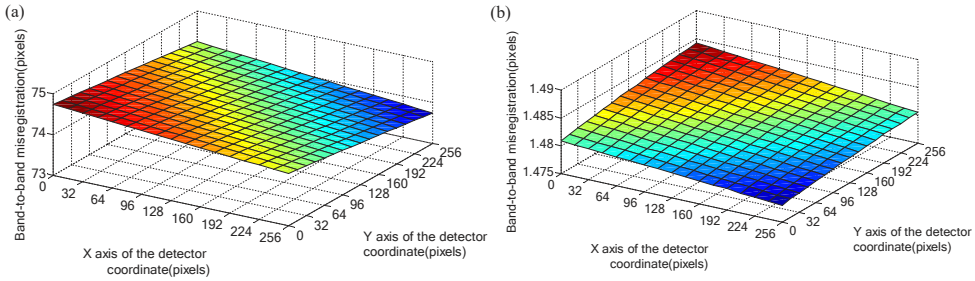

Fig. 4. (a) Band-to-band misregistration between first band and last band. (b) The number of blurred pixels in the first band.

In summary, in order to extensively meet the observation requirements in different scenarios and platforms, it is necessary to solve the image blur problem for an AOTF imaging spectrometers with long integration time. The objective of this work is to further develop and verify the image restoration ability of dual-path architecture in spectral image restoration. The first section has simulated and summarized the difficulties in the space application of AOTF imaging spectrometer. Then, Section 2 will describe the concept of dual-path system for spectral image restoration. After that, Section 3 will emphasize a study of motion kernel generation, which is based on a undiffracted image detection technique. Ultimately, the experiment in Section 4 will prove the method used in this paper could achieve accurate and robust spectral image restoration.

2. AOTF dual-path system for spectral image restoration

In order to improve the blurred spectral image restoration ability of the dual-path architecture, a laboratory prototype is built, shown in Fig. 5. The incident light from objects is collimated by a telescopic system, ordinary polarized by a polarizer, and passed through an AOTF. The AOTF fabricated by Gooch & Housego Corp. covers the wavelength ranging from 550 nm to 1000 nm with spectral resolution less than 8 nm. A wire grid polarizer supplied by Moxtek Corp. is used to separate the extraordinary diffracted ray and the ordinary undiffracted beam behind AOTF. A doublet prism is used to correct chromatic aberration in the extraordinary diffracted path. These two beams are then focused by two optical lenses, and reimaged onto two detectors separately. When platform vibrates, the undiffracted beam and diffracted beam encounters the same image shifts. In addition, since the panchromatic undiffracted image is formed as multiple monochromatic images overlapped together, its energy is much stronger than the diffracted beam. The ratio of energy between undiffracted image and diffracted order will exceed 100 times, calculated when the AOTF's average spectral resolution is 5 nm with a wavelength range of 700 nm. As a consequence, the undiffracted beam path is a natural and high SNR motion detection channel, since the exposure time of CMOS detector in undiffracted path can be much shorter than the diffracted path. Thus, using multiple sequent short-exposure-time undiffracted images, the blurred kernel of diffracted spectral images can be reconstructed.

In order to ensure that the undiffracted channel accurately reflects the dynamic image shift of the diffracted path, two global shutter CMOS cameras embed with MT9V024 are selected, which also have external triggering capability. Then, the AOTF's RF driver, short-exposure camera and long-exposure camera are all controlled by synchronous external triggering signal. The specific trigger waveform is shown in Fig. 6. Because the AOTF's RF driver trigger and diffracted path detector trigger have the same waveform, they can be triggered together by a same signal using a SMA tee adapter. Therefore, these three trigger signals can be generated by a dual-channel arbitrary /function generator such as AFG3252 from Tektronix.

Optics EXPRESS

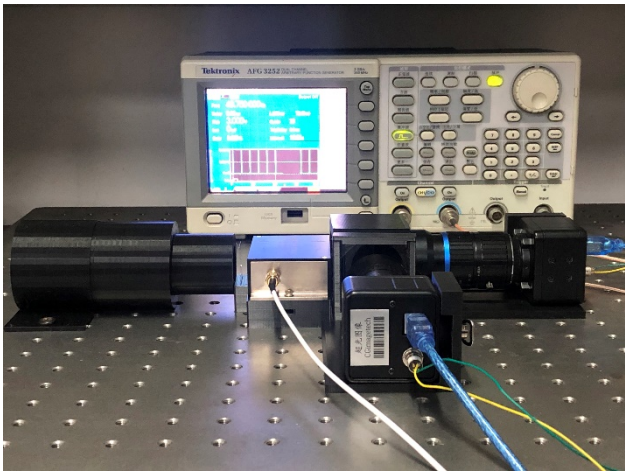

Fig. 5. Laboratory prototype of dual path AOTF imaging system for spectral image restoration.

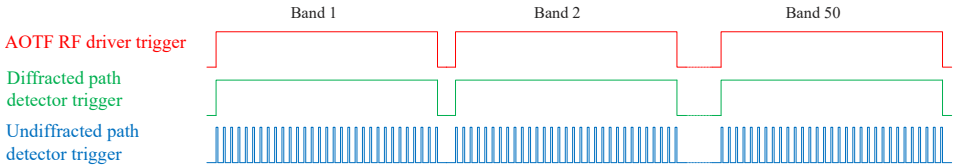

Fig. 6. External trigger waveform for RF driver and two detectors.

3. Calibration of dual-path image motion measurement

In order to measure image motion accurately, the first step is to guarantee that total acquisition time of multiple short-exposure images is the same as the integration time of the long-exposure blurred spectral image. However, the preset value of the exposure time displayed on the camera operation interface may be substantially different from the actual value. Therefore, Fig. 7 has demonstrated an installation of calibrating the integration time. Firstly, a DC gear motor is placed in front of the dual-path system as the calibration target. A 3D printed long strip with a 0603 SMD LED is mounted on the rotating shaft of the motor. The green LED is chosen because it is within the spectral range of AOTF. In addition, it is visible light, readily available and easy to observe with the naked eye. On the back of the long strip, we embedded two 1.5 V button cells. They are connected in series to power the LED. Therefore, the button cells and LED will spin together, and the power wires will not be entangled. Meantime, a PWM driver board, powered by linear DC regulated power supply, is used to control and adjusts the rotation speed of the motor. After the motor drives the LED to rotate, it will form a bright circle with a stable rotation speed, and the rotation period can be adjusted by the driver board.

Therefore, when the exposure time of detector used in diffracted path equals to the LED rotation period, a uniform and complete white bright circle will be imaged, as shown in Fig. 8(a). When the exposure time is less than the rotation period, a gap will appear in the bright circle, shown in Fig. 8(b). Otherwise, if the integration time is longer than the rotation period, some areas of the bright circle will be significantly brighter.

On the other hand, the time when the short-exposure undiffracted path starts to acquire images is determined by the rise trigger edge. Then, when the LED is rotating, the image captured by the short exposure camera will be bright spots at different positions on a circle. In addition, the

Optics EXPRESS

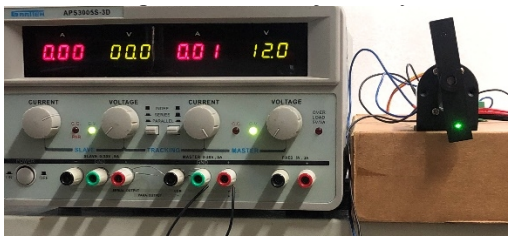

Fig. 7. The setup to calibrate the integration time of dual-path system.

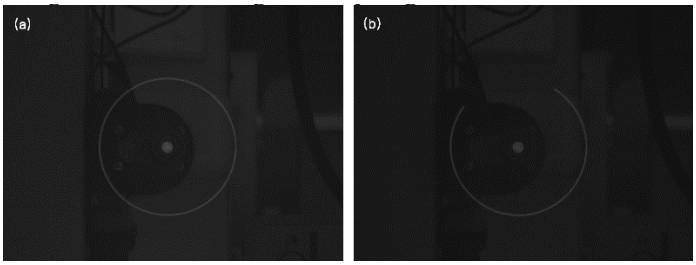

Fig. 8. (a) A complete white bright circle presents when the exposure time of detector equals to the LED rotation period. (b) An uncomplete circle with a gap presents when the exposure time of detector is less than the LED rotation period.

time interval between the first pulse rising edge and the last pulse rising edge should be equal to the exposure time of the diffracted path's detector, which will also be the same as the LED rotation period. Therefore, the positions of the bright spots captured at the first trigger pulse and last trigger pulse will have the same coordinates. Since the trigger period and exposure time can be tuned finely, the pixel number of circle gaps (or overlaps) and spots coordinates difference can be adjusted to less than 2 pixels in our experiments. So divided by the number of pixels corresponding circumference of a circle, the two path's exposure time difference is not more than 0.5‰, which guarantees high blur kernel calculation accuracy.

The next step is to calibrate the spatial relationship of the two paths. A dot grid calibration target is used to adjust two optical paths coaxially, and the residual error can be calculated based on the extraction of the center of the circles. Figures 9(a) and 9(b) have shown the images of calibration board captured by the undiffracted and diffracted optical channels respectively, when AOTF is tuned to 750 nm. Local weighted mean (LWM) [8] models with second-order polynomial functions are used to fit their transformation. The two images have presented a certain difference in resolution, mainly due to the lens chosen possessing a slightly longer focal length in the non-diffraction light channel, which can improve the accuracy of image movement measurement. In aerospace applications, the on-orbit calibration of the spatial relationship between two channels can be operated by pointing the dual-path system to stars.

Optics EXPRESS

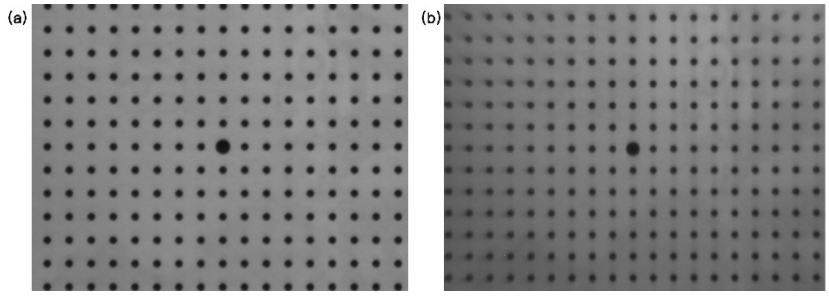

Fig. 9. (a) The image of calibration board captured by the undiffracted path. (b) The spectral image of calibration board at 750 nm.

4. Experiment setup

In this experiment, a colored cardboard illuminated by a halogen tungsten lamp is used as the target. The cardboard is cut from a packing box of snacks gifts from Thorlabs. A two-dimensional platform driven by two stepper motors, takes the cardboard to move along an arbitrary path, shown in Fig. 10. The motor rotation speed for integration time calibration is set to 102.9 r/min. The integration time of the diffracted path sensor is as long as 583 ms, and the exposure time of the undiffracted path sensor is set to 2.7 ms.

Fig. 10. A colored cardboard carried by two-dimensional platform is used as the target.

During the continuous motion of the cardboard, spectral images from 700 nm to 960 nm are acquired by dual-path system at 10 nm intervals. At the same time, 30 frames of short-exposure images are collected simultaneously within the integration time of collecting each spectral image. Figures 11(a) and 11(b) presents the blurred spectral image at 750 nm and the corresponding 30 frames of undiffracted short-exposure images respectively. The spectral image has been flipped horizontally to keep the same orientation as the undiffracted light images. The size of the blurred spectral image is 640×480 pixels. In order to improve the frame rate of undiffrated path, this experiment has utilized the ROI mode of CMOS, solely capturing the center area of 250×250 pixels.

Then, the first frame of the 30 undiffrated images is used as the reference image, and the relative displacements of the subsequent image and the first frame image are calculated using edge-based phase correlation algorithm [9,10]. Using the calibrated spatial relationship of the two paths, the relative displacements are then transformed to image space of diffracted path. Since the image motion is a two-dimensional vector in the XY image coordinate system, spline

Optics EXPRESS

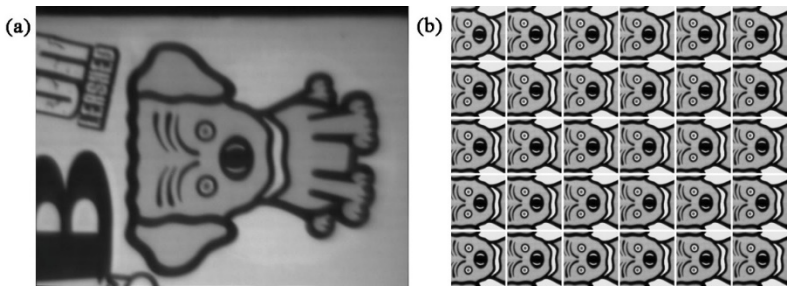

Fig. 11. (a) The blurred spectral image at 750 nm. (b) The corresponding 30 frames of undiffracted short-exposure images.

interpolation for displacement is conducted in the X and Y directions, respectively. Thus, the position of the diffracted image motion trajectory at different subdivision moments is obtainable. Finally, the actual blur kernel is acquired by sampling the motion trajectories on a discrete grid using subpixel linear interpolation, which is shown in Fig. 12(a).

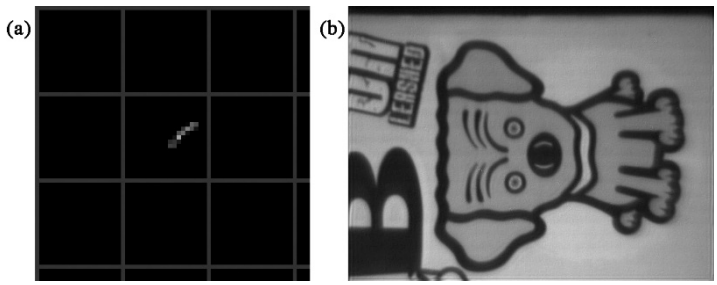

Fig. 12. (a) The blur kernel of spectral image at 750 nm, with grid lines spaced every 20 pixels both vertically and horizontally. (b) The deblurred result of spectral image at 750 nm using the corresponding blur kernel.

The Lucy-Richardson deconvolution algorithm is applied for spectral image restoration, and the deblurred image is shown in the Fig. 12(b). The result shows that the quality of spectral image has been greatly improved, which proves that dual-path system helps to solve the motion blur problem of AOTF imaging spectrometer at a long exposure time. We calculated the PSF blur kernel for all bands, and the results are shown in Fig. 13. After that, we have composed an image sequence using the respective first short-exposure images in each band sampling period, and have computed their image offsets. Figure 14 shows the shifts between the first frame and other images in this image sequence, which can be used as the band-to-band displacements for subsequent calculations. In this experiment, we manually control the output of the trigger signal. When one band is collected, we will turn off the output of the arbitrary generator for a period of time. After the image has moved a long distance, we will turn on the trigger signal to collect the next band. Therefore, there are some large image shifts in Fig. 14, which assists to better evaluate the performance of our method under large spectral misregistration. Figure 15 shows the restored bands after successively performing band-to-band registration and deblurring on the blurred spectral images.

Furthermore, the restoration performance of spectral data cube is evaluated compared with the long-exposure-time data captured when the platform is not moving. We have targeted the center pixel of the dog's right eye and calculated its spectral curve under different conditions, as shown in Fig. 16. The black curve represents the correct spectral data at the center of the

Optics EXPRESS

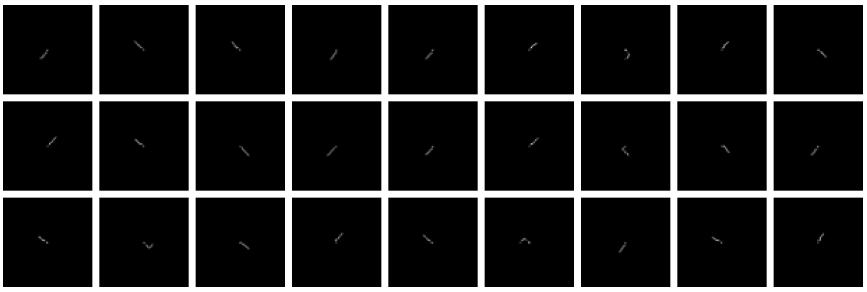

Fig. 13. The corresponding blur kernel of blurred spectral images from 700 nm to 960 nm.

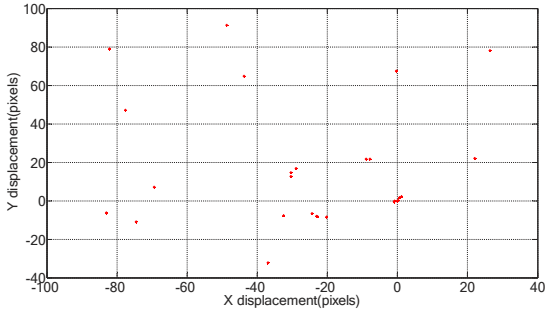

Fig. 14. The band-to-band displacement is calculated using each first undiffracted short-exposure images in 27 spectral bands acquisition period.

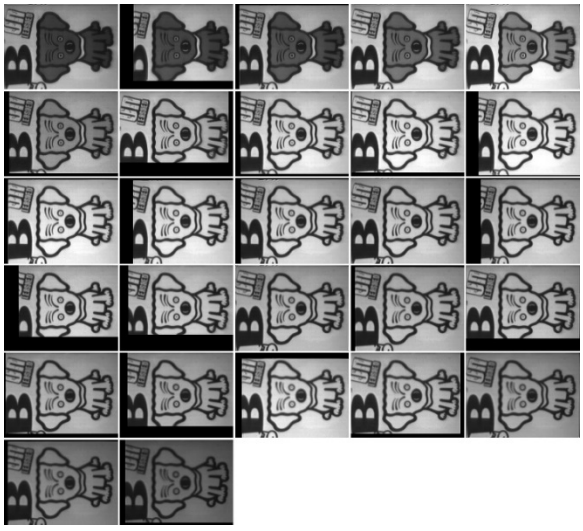

Fig. 15. The deblurred result of spectral images from 700 nm to 960 nm.

Optics EXPRESS

cartoon dog's eyes on stationary platform. The blue curve represents the incorrect spectral data extracted from the eyes' center pixel, which is extracted from the (314, 193) coordinates of the raw spectral image data cube. In the first band, this point is exactly the center of the dog's right eye. This relatively large error from the correct spectrum is not only caused by band mismatch, but also errors caused by spectral image blurring. The red band-to-band registrated spectrum curve is obtained by using the relative displacements of Fig. 14 to process the original spectral data cube. This curve is also extracted from the (314, 193) coordinates in the images. It can be seen that there is still an obvious difference between this curve and the black curve. An obvious reason is that image blurring changes pixel values. Another reason is that the blur PSFs of each band are different, resulting in inaccurate band-to-band registration. The green curve represents the spectral data after band-to-band registration and spectral image deblurred, which is very close to the correct spectral curve. This curve is extracted from (318, 196) coordinates of all the restored spectral images. The reason for the different coordinates is that each band image has been deblurred, so its eye center coordinates have changed and need to be retargeted. From this comparison, the feasibility of this method is clearly illustrated.

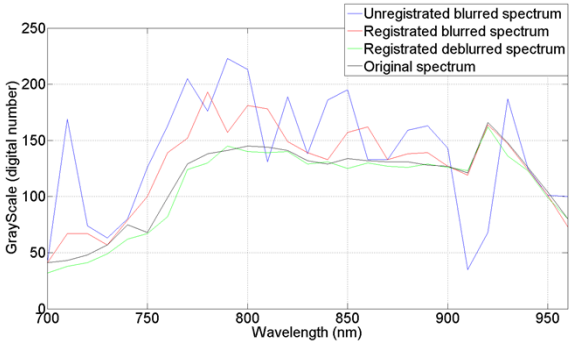

Fig. 16. A comparison between the original correct spectrum, unregistered blurred spectrum, registered blurred spectrum and registered deblurred spectrum.

Another concern is that the grayscale and PSF of each band are often different. When the image brightness is stronger or the blurred shift is larger, less iterations is beneficial for reducing ring artifacts in deblurred images. The optimal number of iterations can also be determined by plotting the curve of SNR and the PSNR as iteration number, and this method will be more intelligent. To simplify, the number of Lucy-Richardson iterations of all bands is set to 7 times, which performs well enough for the current experimental data.

5. Conclusions

In this paper, we first summarized and modeled the possible observation modes that AOTF can employ in space. It was discovered that the problem of spectral images blur is crucial, when AOTF image spectrometer is used in GEO observation and specified areas pointing from AEOS. This paper also demonstrated that spectral image blur not only caused image quality degradation, but also reduced the credibility of band-to-band registration. If the remaining image blur problem could be solved, it would greatly expand the practical application scope of AOTF. Therefore, it proposed a dual-path architecture solution for spectral image deblurring, and built a laboratory prototype. After that, the integration time calibration and the dual path image calibration were proposed and conducted. Then, the image blur kernel of the spectral image can be precisely obtained by using the sequential short-exposure undiffracted beam images, which benefits from the high brightness of undiffracted path and the consistency of image shift with diffracted path. Ultimately, the spectrum restoration experiment shows that this method contributes to

Optics EXPRESS

the reliability and accuracy for images restoration and band-to-band registration. This paper focuses on the case of overall uniform image blur caused by platform motion. In another situation when the platform and a small target in the scene are moving in different trajectories at the same time, we believe that the proposed method is still applicable. First, since the target is relatively small compared to the scene, traditional image registration methods such as phase correlation algorithm can be used to calculate the displacements of the short-exposure-time undiffracted images. Therefore, the blurred PSF of the background can be obtained. Then, after registering all the undiffracted images with the calculated displacements, a moving target detection algorithm such as image background subtraction can be used to extract the position of the small target at different times. After that, the blur kernel of the small target can be obtained. Finally, the different regions of the blurred spectral image can be deblurred separately using the background PSF and the small target PSF. We will verify this idea in our future work. Therefore, the accomplishment of this paper provides significant technical support for the aerospace application of AOTF image spectrometer.

Funding. National Natural Science Foundation of China (62075202); Natural Science Foundation of Zhejiang Province (LY20F050008); Open Foundation of the Key Laboratory of Aeronautical Optical Imaging and Measurement, Chinese Academy of Sciences; Fundamental Research Funds for the Provincial Universities of Zhejiang.

Disclosures. The authors declare no conflicts of interest.

Data availability. Data underlying the results presented in this paper are not publicly available at this time but may be obtained from the authors upon reasonable request.

References

1. I. Chang, "Acousto-optic tunable filters," Opt. Eng. **20**(6), 824–829 (1981).
2. J. Li, Y. Gui, R. Xu, Z. Zhang, W. Liu, G. Lv, M. Wang, C. Li, and Z. He, "Applications of AOTF spectrometers in in situ lunar measurements," Materials **14**(13), 3454 (2021).
3. H. Zhao, P. Zhou, Y. Zhang, Z. Wang, and S. Shi, "Development of a dual-path system for band-to-band registration of an acousto-optic tunable filter-based imaging spectrometer," Opt. Lett. **38**(20), 4120–4123 (2013).
4. P. Xie, H. Wang, Y. Chen, and P. Wang, "A heuristic algorithm based on temporal conflict network for agile Earth observing satellite scheduling problem," IEEE Access **7**, 61024–61033 (2019).
5. J. J. Puschell and P. A. Tompkins, "Imaging spectrometers for future earth observing systems," Proc. SPIE **3117**, 36–48 (1997).
6. M. Katayama, Y. Suzaki, S. Aso, and H. Hirayama, "Attitude Control Simulator for the Small Satellite and Its Validation by On-orbit Data of QSAT-EOS," presented at the *31st Annual AIAA/USU Conference on Small Satellites*, Logan, Utah, USA, 5-10 August 2017.
7. D. G. Lowe, "Distinctive Image Features from Scale-Invariant Keypoints," Int. J. Comput. Vis. **60**(2), 91–110 (2004).
8. A. Goshtasby, "Image registration by local approximation methods," Image Vis. Comput. **6**(4), 255–261 (1988).
9. H. Foroosh, J. B. Zerubia, and M. Berthod, "Extension of phase correlation to subpixel registration," IEEE Trans. Image Process. **11**(3), 188–200 (2002).
10. R. Liang, B. Zhang, X. Gong, M. Chen, J. Zhang, Y. Hu, Z. Wang, and J. Qian, "Jitter correction for EAST infrared videos using edge-based phase correlation method," Fusion Eng. Des. **176**, 113035 (2022).